Interface modification for enhancing the conduction mechanisms in 2,2',7,7'-tetrakis(N,N-diphenylamine)-9,9'-spirobifluorene (Spiro-TAD) Nano layers for optoelectronic applications

Omwati Rana, Ritu Srivastava, M.N.Kamalasanan, M.Husain, M.Zulfequar

Abstract— ***Hole transport properties of 2,2',7,7'-tetrakis(N,N-diphenylamine)-9,9'-spirobifluorene (Spiro-TAD) have been analyzed by studying the J-V characteristics of hole only devices at different temperatures and nano layer thicknesses of Spiro-TAD in the devices. The conduction processes were understood by using Richardson Schottky (RS) thermionic model and found injection limited behaviour. When an optimised nano layer of F4TCNQ was inserted between the organic layer and metal electrodes, the injection energy barrier at metal/organic interface was found to reduce significantly. By the optimised nano layer of F4TCNQ, completely removal of interface barrier is possible. It has been observed that the J-V characteristics of interface modified devices were well fitted through space charge limited conduction (SCLC) with electric field and temperature dependent charge carrier mobility model. The obtained values of hole mobility by varying electric field and temperatures were well fitted with both Gill's model as well as Gaussian disorder model within the experimental accuracy. Mobility parameters obtained from J-V measurements were comparable to those reported from Time of flight (TOF) technique and field effect transistors (FETs) measurements. These results show that it is possible to tune the conduction mechanism in various optoelectronic devices by modifying their interfaces and remove interface barriers which are detrimental to the efficiency and stability of these devices.***

Keywords: Charge Transport; Injection Limited Conduction; SCLC; Hole Mobility; Gills Model; Gaussian Disorder model

1. INTRODUCTION

During few decades, Organic semiconductors have covered a broad range of electronic devices because of ability to manufacture large area and flexible devices at very low cost. All electronic devices like light emitting diodes (LEDs), field-effect transistors (FETs), photovoltaic's (PVs), lasers, sensors, memory chips and integrated circuits [1-7] are included in this range. As huge amount work has been done on organic devices for technological and commercial applications. Still there are major issues related to controlling the lifetime and reproducibility of these devices.

Performance and life time of an organic device basically depends upon major three factors: as i) the efficiency of charge carriers injection/extraction from electrodes to organic layers [8-9] ii) Charge carrier mobility of materials [10] iii) Morphological stability of organic layers (which require high glass transition temperature ($T_{g)}$ organic materials)[11]. In order to fulfil these requirements, thermally stable with high charge carrier mobility organic materials should be develop which having good injection efficiency at the interfaces.

As a result, many structural modifications have been done through in developing new organic materials which possessing high glass transition temperature (T_g)[12-13]. One of the good quality approach introduced by Salbeck and group by introduction of Spiro-type linkages, making covalently bridged orthogonal structural configurations which can reduce crystallization tendencies efficiently which leading to exhibiting higher values of Tg without influencing the mobility of materials [14-15]. For example, while linking two charge transport moieties (for instance, two identical TAD, TAD stands for *N,N,N',N'* tetraphenylbenzidine) through a spiro-carbon centre resulting spiro-compound, 2,2',7,7' tetrakis(diphenylamino)-9,9'-spiro-bifluorene (Spiro-TAD) with raising the glass transition temperature T_g $=70^0$C (TAD) to 133^0C(Spiro TAD) due to the increase in steric demand and effectively hinders crystallization[16]. Because of thermal stability, spiro linked compounds found applications in various organic devices i.e solar cells, OLEDs and TFTs [17-19].

Further, in organic devices, Injection of charge carrier at the interfaces (anode/organic layer or organic layer/cathode) mainly controls by the alignments of energy-level at the

Revised Version Manuscript Received on March 08, 2019.

Omwati Rana, Department of Physics, Daulat Ram College, University of Delhi and Advanced Materials and Devices Division, CSIR-National Physical Laboratory and Department of Physics, Jamia Millia Islamia, Jamia Nagar, New Delhi, India.(e-mail: omkhtr@gmail.com)

Ritu Srivastava, Department of Physics, Daulat Ram College, University of Delhi, Delhi, India

M.N.Kamalasanan, Department of Physics, Daulat Ram College, University of Delhi, Delhi, India

M.Husain, Advanced Materials and Devices Division, CSIR-National Physical Laboratory, Dr. K. S. Krishnan Road, New Delhi, India

M.Zulfequar, Advanced Materials and Devices Division, CSIR-National Physical Laboratory, Dr. K. S. Krishnan Road, New Delhi, India

*Published By:
Blue Eyes Intelligence Engineering
& Sciences Publication*

International Journal of Recent Technology and Engineering
IJRTE
www.ijrte.org
Exploring Innovation

interfaces. Lowering of energy barrier at the interfaces is important to improve the efficient charge injection through the interfaces. The appropriate approaches to reduce the injection barrier for carriers are either by inserting a nano layers (organic or inorganic materials) in between the interfaces or using the doped charge transporting organic layers in the device [20-22]. A range of inorganic/ organic materials such as WO_3, MoO_3, F_4TCNQ, ReO_3, LiF, and Cs are available which can be introduced as interface layers or dopants in various hole transporting materials for improvement of optoelectronic devices [22-24]. After injection of charge carrier requirement of the organic materials must also possess high mobility of transferring the charge carriers through the devices. It has been widely agreed that the charge-carrier mobility μ is one of the most important quantities and it is important to understand how μ depends on various device parameters [25-26]. Numerous studies show, the dependence of the mobility μ on temperature *T,* electric field *E* and charge carrier has been extensively investigated by various charge transport models as Gill's Model, Gaussian Disorder Model (GDM) etc. [27- 29].

In present investigation, we have selected a well known hole transporting material Spiro-TAD which has been used in OLEDs [30-31], OFET, organic phototransistors (OPT) and OPVs [32]. Spiro TAD is a morphologically stable (T_g = 133^0C) material with the good hole mobility μ ~ 2-8 $x10^{-4}$ $cm^2V^{-1}s^{-1}$ (measured by TOF and EFT methods) [33]. Its molecular structure can be seen in Figure 1.

In the report, we have focused on the SCLC method to evaluate the hole mobility of Spiro TAD films by using J-V Characteristics, as very little experimental evidences are available in this regard. Although the SCLC theory has been well established but the mobility analyses of organic semiconductors have rarely been used because the basic requirement of a good Ohmic contact at the metal/organic interfaces [34]. We have measured the J-V characteristic by fabricated hole only devices ITO/Spiro TAD/Au with varying the thicknesses and temperature. From J-V measurements, Injection limited behaviour has been observed. To make ohmic contact between ITO/Spiro TAD, most prominent electron acceptors is 2,3,5,6-Tetrafluoro-7,7,8,8,- tetracyano-quinodimethane (F_4-TCNQ), has been used as a interface layer. First, we have optimized the F_4TCNQ thickness and it was found that at 7nm thickness of F_4TCNQ, the J-V characteristics of the device ITO/F_4TCNQ (7nm)/Spiro TAD(250nm)/F_4TCNQ (7nm)/Au, show ohmic contact at interface, then space charge limited current which enable us to measure the hole mobility with varying electric field and temperatures. The obtained structural parameters which derived by fitting measured mobility values in existing mobility models as Gills and GDM are comparable with the results obtained from TOF and FET technique.

2. EXPERIMENTAL DETAILS

Indium Tin Oxide glass(ITO) (thickness ~ 120 nm, sheet resistance 20 Ω/□) substrates which were pre cleaned by successive ultrasonic treatment for 20 min in acetone, trichloroethylene and isopropyl alcohol were used to fabricate the hole only devices. For enhancing the work function of ITO substrates, the surfaces of ITO substrate were treated with oxygen plasma for 5 minutes. Then hole only samples with the device structure ITO/ Spiro TAD (x nm)/ Au were fabricated for different thicknesses (x=150nm, 200nm, 250nm) and temperatures (300K-145K). Modified interface hole only devices were also fabricated with the device structure ITO/F_4TCNQ(y nm)/Spiro TAD(250 nm)/F_4TCNQ(y nm) /Au for different thicknesses of F_4TCNQ (y =1, 3, 5, 7 nm) and temperatures (300K-145K). High vacuum of range 10^{-5}-10^{-6} torr has been used for deposition of Organic materials onto ITO substrates at the rate of deposition of 0.4Å/s and the Au (500nm) electrodes were deposited without breaking the vacuum. Thicknesses of the deposited layers were monitored by using the in situ quartz crystal thickness monitor. The size of each device was 4mm x 4mm. Before doing the measurement the fabricated devices were encapsulated with epoxy in a dry nitrogen glove box. Then J-V characteristics of the fabricated devices were measured by using a keithley 2610 source measurement unit that interfaced with a computer.

3. RESULTS AND DISCUSSION

a) Injection limited conduction mechanism in pure Spiro TAD

Figure 1 shows the systematic diagram with energy levels of fabricated devices in which Spiro-TAD is sandwich between ITO(anode) and Au(cathode) electrodes, with varying thicknesses as 150nm, 200nm and 250nm. From energy level diagram, the work function of ITO is about 4.8 eV and the Highest Occupied molecular orbit (HOMO) value of Spiro TAD is 5.4 eV [36]. The barrier is ~0.6eV for hole injection from ITO to Spiro TAD and 2.4 eV for electron injection from ITO to the lowest unoccupied molecular Orbital (LUMO) of Spiro TAD. Therefore, ITO/Spiro-TAD/Au is a hole (single carrier) transporting device.

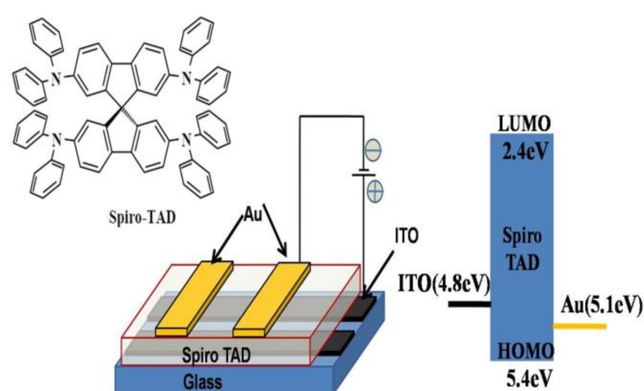

Figure 1.The systematic diagram of hole only device of spiro TAD with energy level diagram and molecular structure of spiro TAD.

International Journal of Recent Technology and Engineering
IJRTE
www.ijrte.org
Exploring Innovation

J-V characteristics of devices with varying thickness of Spiro-TAD at room temperature are shown in inset of Figure 2 which shows current density (J) increases nonlinearly with voltage (V). It also show the variation of current density (J) vs electric field (F) in semi logarithmic scale to distinguish the conduction mechanism in the Spiro -TAD.

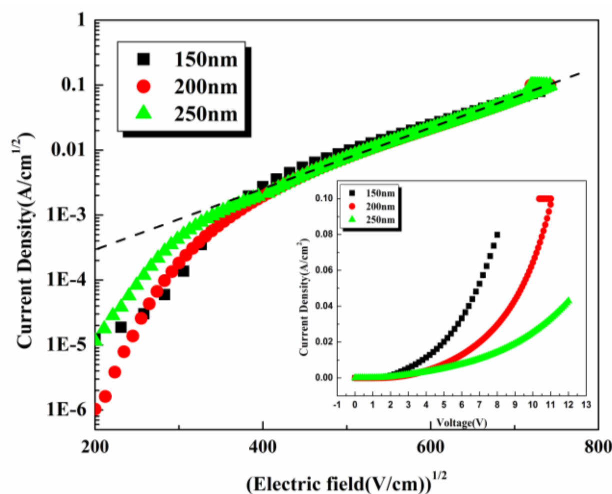

Figure 2: Current Density(J)- Electric field(F) characteristics of Spiro TAD devices as varying the Spiro -TAD layer thicknesses in semi logarithmic scale and J-V characteristics of devices at room temperature in the inset (linear scale).

As W. Brutting et al reported distinctive criterions to distinguish between injection or bulk limited behaviour using thickness dependence of J-V characteristics of device [37]. For purely injection limited behaviour, plot of log(J) versus $\sqrt{F}$ should be independent of organic thickness and show linear dependency. It has been observed from Figure. 2, injection limited conduction is the prominent charge transport mechanism in the current case. Basically in injection limited conduction charge carriers face the barrier at the interface of metal electrode/organic layer may be due to mismatch of energy levels, in this case injection occur through via quantum mechanical tunnelling through the potential barrier (Fowler Nordheim (FN) tunnelling) . On other side, in small barriers or ohmic contact at interface, a large number carriers easily cross the barrier due enough thermal energy to cross the barrier (Richardson Schottky (RS) thermionic emission) [38]. As device show injection limited conduction, to measure the barrier, Temperature-dependent electrical characteristics are used.

Figure 3(a) show, *J-V* characteristics of device ITO/Spiro-TAD (250nm)/ Au. It is observed from the J-V characteristics, as temperature and voltage increase current also increase nonlinearly, show RS thermionic type of injection mechanism. Variations in J-V with temperature discarded F-N tunneling mechanism. The Richardson–Schottky (RS) thermionic emission model in which the relation between J and electric field (F) can be written in the form [39]

$$J_{RS} = A^* T^2 \exp \frac{-(\varphi_b - q\sqrt{\frac{qF}{4\Pi\varepsilon\varepsilon_0}})}{kT} \quad - (1)$$

Where A* is the Richardson constant (A^*=120) and m^* (effective carrier mass), T is the absolute temperature, ϕ_b is barrier height, k is the Boltzmann's constant, q is electric charge of holes, ε the dielectric constant and ε_0 is the permittivity of free space.

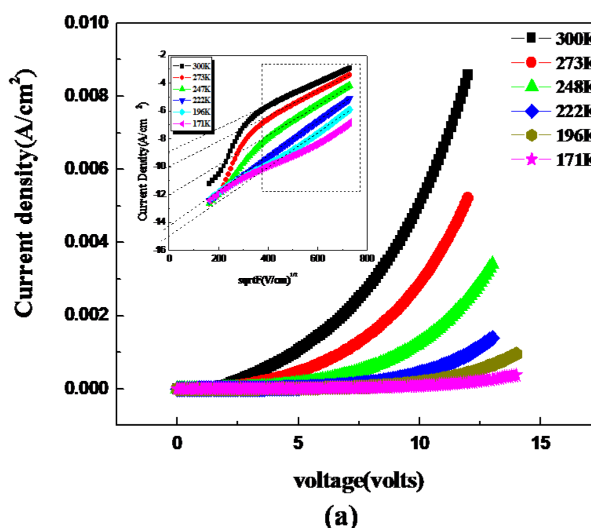

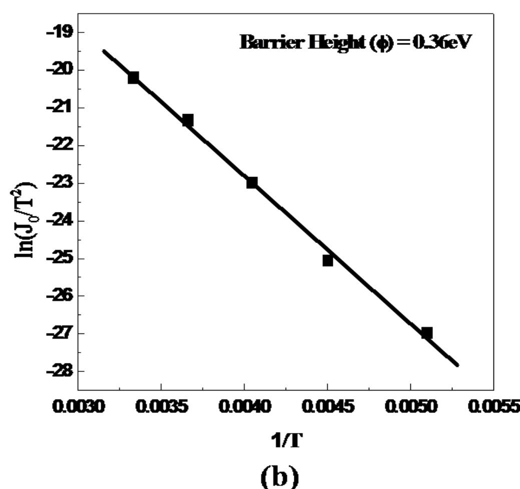

Figure 3 (a) J-V characteristics of device with varying temperatures (linear scale). Inset show plot of lnJ vs sqrt F of device indicating RS type injection mechanism and the dotted lines shows the value of zero current density at different temperature. (b) The plot of $\ln(J_0/T^2)$ vs. 1/T for calculating the barrier height of ITO/Spiro TAD interface.

In RS mechanism, ln J shows linear dependence on √F (from eqn 1). It is clearly observed from inset of Figure 3(a) that current density(J) obey such a linear dependence on √F at higher field (shown the area enclosed in square) and deviate from the linear behaviour at low electric field. This deviation may be due to leakage current [40]

From equation 1, When F =0 V/cm, J_0 is the Zero field current density, then

Published By:
Blue Eyes Intelligence Engineering
& Sciences Publication

$$\ln\left(\frac{J_0}{T^2}\right) = \ln\left(A^*\right) + \left[\left(-\frac{\Phi_b}{k}\right)\right]\frac{1}{T} \quad - (2)$$

J_0 can measure by extrapolating current densities at different temperature to zero electric field. The value of barrier height (Φ_b) at interface can be determined by plotting $\ln(J_0/T^2)$ vs. 1/T which is a straight line shown in the Figure 3(b). Slope of which gives $-(\Phi_b/k)$ from which Φ_b has been calculated. The calculated potential barrier is 0.36 eV.

(b) Optimisation of F4TCNQ as interface layer

To reduce the barrier height between ITO/Spiro TAD and Au/Spiro TAD interfaces, we have used nano layer of F_4TCNQ at the metal /organic contacts. The systematic diagram of modified device configuration ITO/F_4TCNQ(x) /Spiro TAD(250 nm)/F_4TCNQ(x)/Au at different F_4TCNQ thicknesses (*x*=1, 3, 5 and 7 nm) and their energy level diagram are shown in Figure 4(a). It is found experimentally that the hole currents of devices with F_4TCNQ layer are indeed dramatically increased with respect to devices without the F_4TCNQ buffer layer as shown in Figure 4(b). The J-V Characteristics of device with 7-nm-thick F_4TCNQ exhibited the highest current density as well as follow square law ($J \alpha V^2$) that indicate device is controlled by space-charge-limited current (SCLC) mechanism (solid line shows SCLC) and show formation of an Ohmic contact at the interfaces.

Braun et al studied that the monolayer of F_4-TCNQ modified the work function of substrates (in range from 3.45 eV to 5.8 eV) upto ~5.5eV and explained it using an integer charge transfer model (ICT). [41].

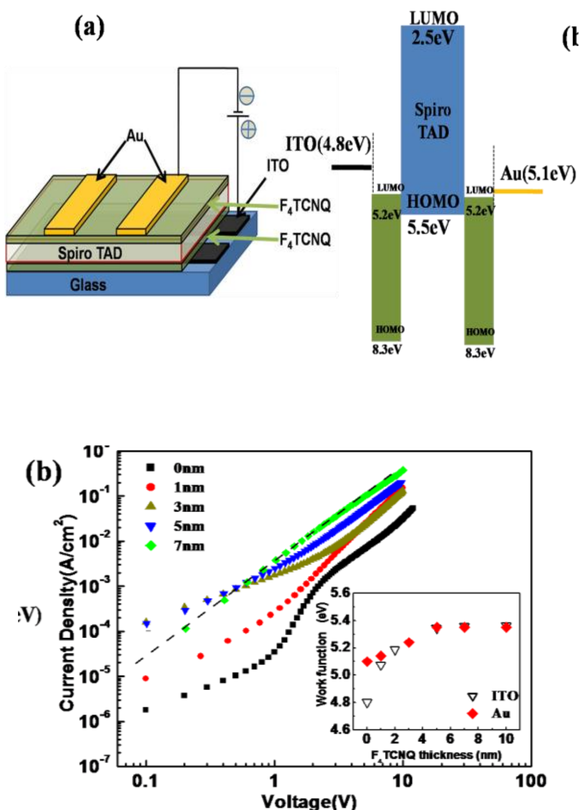

Figure 4.(a) *The systematic diagram of device of spiro TAD with modified electrodes using thin layer of F_4TCNQ and energy level diagram of the device .(b) J-V characteristics of device with configuration ITO/F_4TCNQ(x nm))/spiro TAD(250nm)/F_4TCNQ(x nm) devices with various thickness of F_4TCNQ(x =0,1,3,5,7nm)as buffer layer. Variation in Work function of ITO,Au with F_4TCNQ thickness shown in inset.*

We have also measured the work function of F_4TCNQ deposited modified substrates using Kelvin probe method. Different thicknesses of F_4TCNQ layers were deposited on ITO and Au coated glass substrates [42]. It is shown in Figure 4(b) the work functions of the ITO and Au substrates increased and then saturate at 5.4eV as the F_4TCNQ thickness [42]. This is matching with HOMO of Spiro TAD (5.4eV) indicating that no hole-injection barrier.

(C) Space-charge-limited conduction in Modified Spiro TAD devices

To study the properties of Spiro-TAD, interface modified devices have been fabricated. *J –V* characteristics of device with configuration ITO/ F_4-TCNQ (7 nm)/Spiro-TAD/ F_4-TCNQ (7 nm)/ Au at various thicknesses of Spiro TAD (150nm, 200nm, 250nm) at room temperature are shown in Figure 5(a). It is observed clearly the curves are not merging to each other while plotting log J vs $\sqrt{F}$ as observed in Figure 2 that means no indication of injection limited behaviour, it shows effect of SCLC. It can be observed by plotting the J-V characteristics in double logarithmic scale, shows a straight line with slope 1.9, 2.0 and 2.1 for different thickness (shown in inset of Fig 5(a)).It is the behaviour of SCLC can explain by using SCLC equation 4.

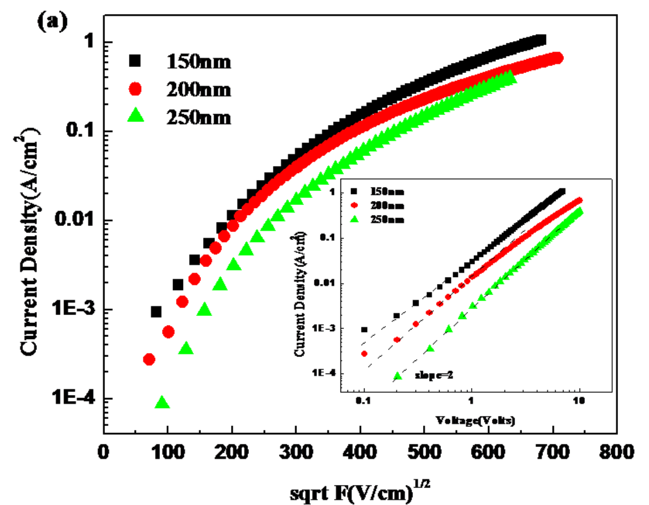

International Journal of Recent Technology and Engineering
IJRTE
www.ijrte.org
Exploring Innovation

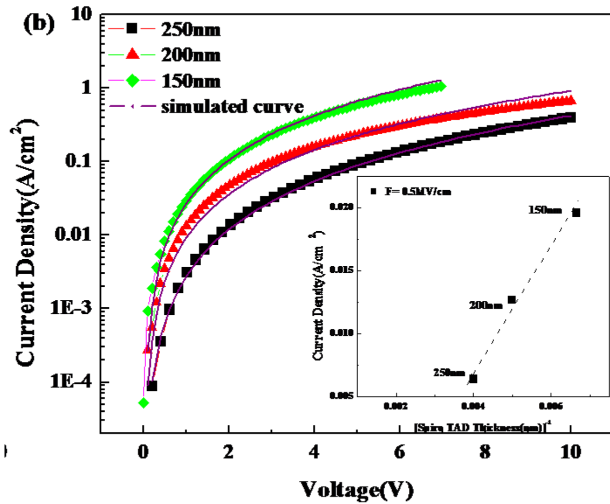

Figure 5.(a) J-V Characteristics of ITO/F_4TCNQ(7nm)/Spiro-TAD/F_4TCNQ(7nm)/Au devices at different Spiro-TAD layer thicknesses and SCLC shown in set . 5(b) J-V characteristics with simulated currents for SCLC with a field dependent mobility. Thickness dependence of the current at a constant electric field of 0.5 MV/cm(shown in inset of figure 5(b))

To have SCLC, at least one contact must be ohmic and injection efficiency (η) should be unity. The injection efficiency of metal /organic semiconductor is defined as the ratio between; the measured current density (J_{INJ}) to the corresponding space-charge-limited current (J_{SCLC}) at a particular electric field as [43].

$$\eta = \frac{J_{INJ}}{J_{TFSCLC}} \qquad -(3)$$

$$J = \frac{9}{8}\varepsilon\varepsilon_0\mu\frac{V^2}{d^3} \qquad -(4)$$

The trap free SCLC equation (4) is given by Mott-Gurney in which charge carrier mobility (μ) independent of electric field and material without intrinsic carriers and traps [44]

As inset of Figure 5(a) shows the J αV^2 upto 2V indicating the effect of space charge in the material. Charge carrier mobility (μ) has been evaluated using equation (4) as $\mu = 1.8\times10^{-4}$ cm^2 V^{-1} s^{-1}. This value is slightly lower than the value of hole mobility reported for Spiro- TAD by Bach et al [33] by the TOF technique which is 2×10^{-4} cm^2 V^{-1} s^{-1}at field 1.6 x10^{-3} V/cm at RT. We also calculate the injection efficiency, it is found to be 0.9 confirming the ohmic contact at interface. As voltage increases, current increases indicating mobility of the charge carrier increases. At high voltages the space charge limited current is described by Murgatroyd eqn -5 in which mobility of charge carriers depends on both the applied voltage and temperature [45]

$$J = \frac{9}{8}\varepsilon\varepsilon_0\frac{V^2}{d^3}\mu(0,T)\exp\left(0.89\gamma\sqrt{\frac{V}{d}}\right) \qquad -(5)$$

In eqn 5, μ(0,T) and γ are the zero field mobility and field lowering factor at T temperature. Figure 5(b) shows J-V data in semi logarithmic scale for thickness d =150, 200 and 250nm compared with numerical simulations using eqn 5 for the SCLC including a field and temperature dependent mobility parameters as μ(0,T) = 1.2x 10^{-4} cm^{2}V^{-1}s^{-1} and γ =1.1x 10^{-3} (cm/V)$^{1/2}$. Simulation of thickness dependence of J-V characteristics indicate that in Spiro-TAD device current is space charge limited with field dependent charge carrier mobility. On the other hand, reconfirming SCLC using eqn 4, it should obey a power law of the form J α F^2/d^l .It is clear seen from the inset of Figure 5(b), that the J at constant F (0.5MV/cm) is proportional to d^{-1}(while plotting J vs d^{-1}, observed slope of 1). This is confirming the behaviour SCLC in Spiro-TAD device [37].

The Temperature dependency, analysis of the J-V characteristics for modified device as ITO/F_4TCNQ (7nm)/spiro TAD (250nm)/F_4TCNQ(7nm)/Au have been studied in temperature range 127K-300K as shown in Figure 6(a). To analyse the J-V data we have use same SCLC with temperature and field dependent mobility model (using eq^n 5). Figure 6(b) shows the experimental data simulated together with numerically calculated J-V curves using different the values of μ (0, T) and γ for all temperatures.

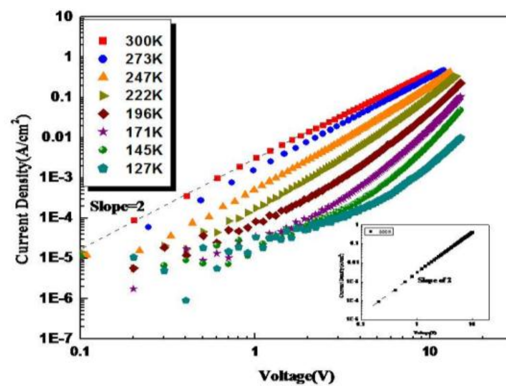

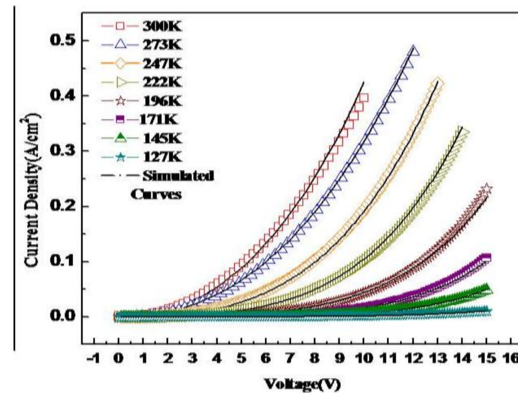

Figure 6: (a) ***J-V characteristics of ITO/F_4TCNQ (7nm)/spiro TAD (250nm)/F_4TCNQ (7nm)/Au hole only devices at different temperatures range(300-127K).Figure 6(b) Shows simulation of the experimental current density(J) with the calculated value of current density using equation (5)***

The obtained values of values of μ (0, T) and γ are plotted with varying temperatures shown in Figure 7 and 8. These types of behaviour as observed in figures (7 and 8) are similar as observed in disordered organic materials. In disordered organic materials, Gill's model [27] and the Gaussian disorder model[17,28] are usually used to explain the temperature and field dependence of the mobility of charge carriers.

In Gill's model, the mobility is given by [27].

$$\mu(F,T) = \mu_0(0)\exp\left(\frac{-\Delta-\gamma\sqrt{F}}{k_B T_{eff}}\right) \qquad - \quad (6)$$

With $\frac{1}{T_{eff}} = \frac{1}{T} - \frac{1}{T_0}$

Where μ0(0) is the zero field mobility at zero temperature, Δ is activation energy at zero electric field, T_0 is an observed parameter. From eqn 6, mobility of charge carriers is proportional to the reciprocal of the temperature (lnμ ~ 1/*T*).

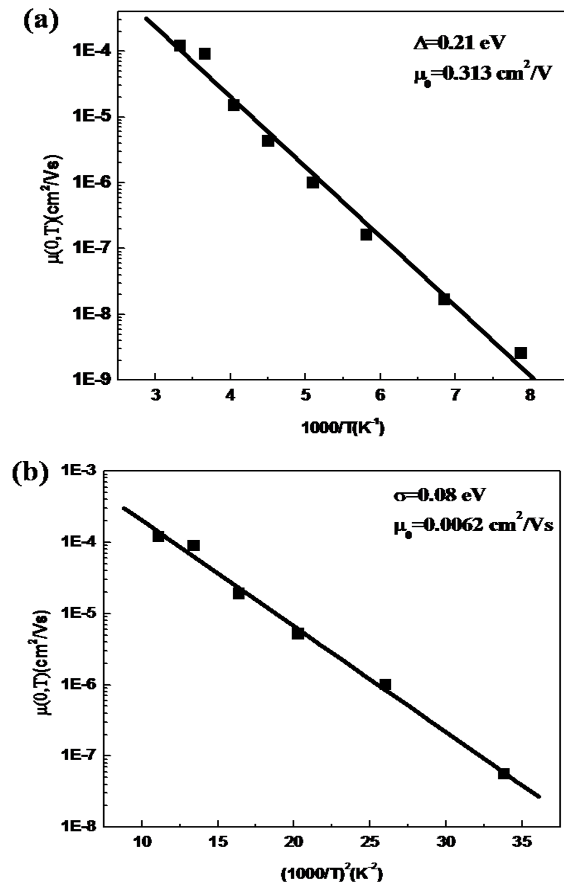

Figure 7: Variation of zero field mobility (μ_0) (a) with 1000/T and (b) with $(1000/T)^2$

Linear dependence has obtained from the plot of ln(μ(0,T) vs 1000/T as shown in Figure 7(a) obtained parameters using eqn (6) are as Δ= 0.21 eV, $\mu_0(0)$=0.313 cm^2/V-sec.

In Gaussian disorder (GD) model or Bässler model [28] mobility is given by equation(7).

$$\mu(T,E) = \mu_\infty \exp\left[-\left(\frac{2\sigma}{3kT}\right)^2\right]\exp\left\{C_0\left[\left(\frac{\sigma}{kT}\right)^2 - \Sigma^2\right]\sqrt{E}\right\} \qquad - \quad (7)$$

σ and ∑ are the energetic and positional disorder parameters respectively among hopping sites of disorder material and μ_∞ is high temperature limit of mobility at zero electric field. Using eqn 7, plot of ln(μ(0,T)) vs. $(1000/T)^2$ in Figure 7(b) which shows the linear dependence to get the value of σ and μ_∞. The obtained values are μ_∞ = 6×10^{-3} cm^2/V.s and σ = 0.08eV. To obtain positional disorder ∑, plot γ versus $(\sigma/kT)^2$ as shown in Figure 8.The obtained values of ∑ and C_0 are 2.22 and 3.86x$10^{-4}$$(cm/V)^{1/2}$ respectively

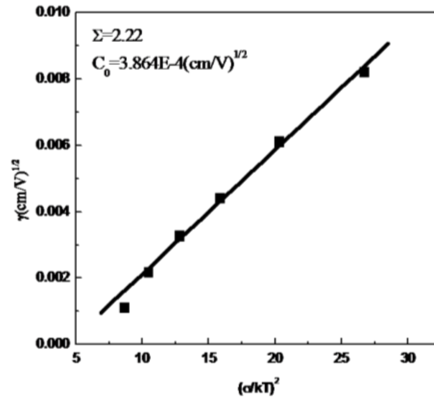

Figure. 8 Plot of coefficient γ against $(1000/T)^2$.

As the temperature range is limited, it is difficult to discriminate Gill and GDM model So, obtained value of mobility from the Gill's model for Spiro TAD ($\mu_0(0)$=0.313 cm^2/V.s) is unexplainably high[46]. In contrast, the mobility obtained from the GDM (μ_∞ = 6×10^{-3} cm^2/V.s), which is comparable for realistic low molar mass amorphous thin films. Then, we can conclude that the analysis based on GDM is more appropriate. It has been observed from Table1 that transport parameters obtained by SCLC technique are comparable to FET and TOF techniques.

Table 1: Summary of the Charge Transport Parameters Obtained by different Techniques

Different Techniques	Gills Model		GD Model			
	μ_0 (cm^2/Vs)	Δ (eV)	μ∞ (cm^2/Vs)	Σ (eV)	∑	C_0 $(cm/V)^{1/2}$
SCLC	0.313	0.21	6.2x10^{-3}	0.08	2.22	3.86x10^{-4}
FET	4x10^{-3}	0.11	4x10^{-4}	0.06	-	-
TOF			0.016	0.08	2.3	2.9 x10^{-4}

Table1. ***Summary of all parameters that have been obtained from SCLC technique and compared with the parameters extracted by FET and TOF techniques [15, 17].***

4. CONCLUSIONS

In this paper, we have described F_4TCNQ used as an interface layer between ITO anode and Spiro-TAD organic layer that improve the conduction mechanism from injection limited to SCLC. As ITO/Spiro-TAD interface is found to be nonohmic contact and show Richardson–Schottky thermionic emission injection and the injection barrier Φ=0.36 eV at the interface. Using an optimized F_4TCNQ layer of 7nm at both interface make ohmic contact and indicating space charge limited conduction (SCLC) mechanism in Spiro-TAD. We are demonstrating that hole mobility and parameters measured by SCLC technique using J-V characterisation measurement in Spiro TAD are comparable to FET and TOF measurements. J-V characterisation require ohmic contact for injection of carriers which reduce loses at the interfaces and improve the efficiency and performance of optoelectronic devices in future.

ACKNOWLEDGEMENTS

The authors are grateful to Council of Scientific and Industrial Research (CSIR)-National Physical Laboratory, New Delhi and University Grant Commission (UGC), New Delhi, for constant financial assistance.

REFERENCES

1. Forrest S R 2004 Nature 428 911.
2. Murphy R and Fréchet J M J 2007 Chem. Rev. 107 1066.
3. Chen Y., Wu X.,. Chu Y., Zhou J., Zhou B., Huang J., 2018, Nano-Micro Lett./doi.org/10.1007/s40820-018-0210-8
4. Gärtner C, Karnutsch C, Pflumm C, and Lemmer U 2007 J. Appl. Phys 101 023107.
5. Frischeisen J, Mayr C, Reinke1 N A, Nowy S and Brütting W 2008 Optics Express 16 18426.
6. Tsujioka T and Kondo H 2003 Appl. Phys. Lett. 83 5.
7. Smits et al 2008 Nature 455 16.
8. Shen Y and Malliaras G G 2000 The Spectrum 13 2.
9. Malliaras G G and Scott J C1998 J. Appl. Phys. 83 5399.
10. Zhao Y S, Fu H B, Peng A D, Ma Y, Xiao D B and Yao J N 2008 Adv. Mater. 20 2859.
11. Salbeck J and Bunsenges B 1996 Phys. Chem. 100 1667.
12. O'Brian D F, Burrows P E, Forrest S R, Koene B E, Loy D E and Thompson M E 1998 Adv. Mater. 10 1108.
13. Oldham W J, Lachicotte R J and Bazan G C 1998 J. Am. Chem. Soc.,120 2987.
14. Salbeck J, Weissörtel F and Bauer J 1997 Macromol. Symp., 125 121.
15. Bach U, Cloedt K D, Spreitzer H and Grätzel M 2000 Adv. Mater 12 14.
16. Mahns B.et al. 2012 J. Chem. Phy. 136 124702.
17. Saragi T P I, Fuhrmann T L and Salbeck 2006 J. Adv. Funct. Mat.16 966.
18. He G, Schneider O, Qin D, Zhou X, Pfeiffer M and Leo K 2004 J. Appl. Phys. 95 5773.
19. Schmidt-Mende L, Kroeze J E, Durrant J R, Nazeeruddin M K and Gra¨tzel M 2005 Nano Lett. 5 1315.
20. Mu-Sen D., X.-Ming W, Lin H Y, Jin Q Q and Gen Y S 2010 Chin. Phys. Lett. 27 12 127802.
21. Wang F X et al 2008 Org. Electron. 9 985.
22. Lee J H, Kim H M, Kim K B and Kim J J 2011 Organic Electronics 12 950.
23. Matsushima T and Adachi C 2008 J. Appl. Phys. 103 034501.
24. Chauhan G, Srivastava R, Kumar A, Rana O, Srivastava P C and Kamalasanan M N 2012 Organic Electronics 13 394.
25. Ambegaokar V, Halperin B I and Langer J S 1971 Phys. Rev. B 4 2612.
26. Baranovskii S D, Zvyagin I P, Cordes H, Yamasaki S and Thomas P 2002 Phys. Status Solidi B 230 281.
27. Gill W D 1972 J. Appl. Phys. 55 12 5033.
28. Ba¨ssler H. 1993 Phys. Status Solidi B 175 15.
29. Pasveer W F, Cottaar J, Tanase C, Coehoorn R, Bobbert P A, Blom P W M, Leeuw D M de and Michels M A J 2005 PRL 94 206601.
30. Winter S, Reineke S, Walzer K and Leo K 2008 Proc. of SPIE Vol. 6999 69992N-1.
31. He G, Schneider O, Qin D, Zhou X, Pfeiffer M, and Leo K 2004 J. Appl. Phys. 95 10.
32. Saragi T P I, Spehr T, Siebert A, Fuhrmann T and Salbeck J 2007 Chem. Rev. 107, 1011.
33. Saragi T P I, Pudzich R, Fuhrmann T and Salbeck J 2002 Mat. Res. Soc. Symp. Proc. Vol. 725.
34. Yasuda T, Yamaguchi Y, Zou D C, and Tsutsui T, 2002 Jpn. J. Appl. Phys., Part 1 41 5626.
35. Chu T Y and Song O K 2007 J. Appl. Phys. 90 203512.
36. Meerheim R, Scholz S, Schwartz G, Reineke S, Olthof S, Walzer K and Leo K 2008 Proc. of SPIE Vol. 6999 699917-1.
37. Brutting W, Berleb S and Muckl A G 2001 Synth. Metals 122 99.
38. Sze S M Physics of Semiconductor Devices, Wiley, New York, 1981
39. Kao H C and Hwang W Electrical Transport in Solids (Oxford: Pergamon) 1981
40. Wand S D, Kanai K, Kawabe E, Ouchi Y and Seki K 2006 Chem. Phys. Lett. 423 170.
41. Braun S and Salaneck W R 2007 Chem. Phys. Lett. 438, 259.
42. Rana O, Srivastava R, Chauhan G, Zulfequar M, Husain M, Srivastava P C and Kamalasanan M N 2012 Phys stat. soldi (a) 1-7 /DOI 10.1002/pssa.201228252.
43. Campbell A J, Bradley D D C and Antoniadis H 2001 J. Appl. Phys. 89 3343.
44. Lampert M A and Mark P Current Injection in Solids, Academic Press, New York
45. (1970).
46. Murgatroyd P N 1970 J. Phys. D 3 151.
47. Ke L., Han R. C. Ch., Vijila C. and Chua S. J. 2007 J Mater Sci 42 9176.